JOURNAL OF AIRCRAFT
Vol. 34, No. 5, September–October 1997

Analysis of the Effect of Sideslip on Delta Wing Roll-Trim Characteristics

Lars E. Ericsson*
Mt. View, California 94040

The effect of sideslip on the roll-trim characteristics around a 30-deg inclined axis has been analyzed for a 60-deg delta wing. By an extension of analytic tools developed earlier for a 65-deg delta wing, the highly nonlinear unsteady aerodynamics can be understood, including the breakaway from one roll-trim condition to another.

Nomenclature

b = wingspan
c_0 = wing root chord
l = rolling moment: coefficient $C_l = l/(\rho_\infty U_\infty^2/2)Sb$
S = reference area, projected wing area
t = time
U = horizontal velocity
x = axial body-fixed coordinate
α = angle of attack
β = angle of sideslip
Δ = increment or amplitude
Λ = leading-edge sweep
ξ = dimensionless x coordinate, x/c_0
ρ = air density
σ = inclination of the roll axis
ϕ = roll angle
$\phi(0)$ = initial roll angle
ϕ_0 = roll trim at $\phi \approx 0$
ϕ_1 = nonzero roll trim

Subscripts
cr = critical
d = discontinuity
s = separation
VB = vortex breakdown
∞ = freestream conditions

Differential Symbols
$C_{l\dot{\phi}}$ = $\partial C_l/\partial(b\dot{\phi}/2U_\infty)$
$\dot{\phi}(t)$ = $\partial\phi/\partial t$
$\bar{\dot{\phi}}$ = $\dot{\phi}b/2U_\infty$

Introduction

THE roll-trim characteristics of a 65-deg delta wing at 30-deg inclination of the roll axis have been investigated extensively.[1–6] Recent tests of a 60-deg delta wing, also at σ = 30 deg, but at nonzero sideslip,[7] have added to the already rich database. The present paper extends earlier analysis[3,4,6] in an effort to pinpoint the flow physics causing the measured multi-roll-trim characteristics of a 60-deg delta wing at sideslip.[7]

Presented as Paper 96-0788 at the AIAA 34th Aerospace Sciences Meeting, Reno, NV, Jan. 15–19, 1996; received Feb. 25, 1996; revision received May 16, 1997; accepted for publication May 27, 1997.

*Engineering Consultant. Fellow AIAA.

Discussion

Figure 1 shows the effect of sideslip β on the roll-trim behavior at σ = 30 deg of a free-to-roll model of a 60-deg delta wing.[7] In addition to changing the trim point ϕ_1, the sideslip changes the roll oscillations from being highly damped for β = 0 and 5 deg to diverge and describe a limit-cycle type of oscillation, commonly known as wing rock, when $\beta > 10$ deg. This paper describes the flow physics generating this effect of sideslip. Figure 2 shows the roll-trim behavior at β = 15 deg for two different release angles: $\phi(0) = 72$ and -52 deg. In the $\phi(0) = 72$ deg case, the roll oscillations build rapidly up to $\Delta\phi \approx 13$ deg around the trim angle $\phi_1 \approx 45$ deg. After 12 cycles, the oscillations break away from $\phi_1 \approx 45$ deg to start describing limit-cycle oscillations of $\Delta\phi \approx 10$ deg around $\phi_1 \approx 18$ deg. In the other case, $\phi(0) = -52$ deg, the behavior is similar. After describing limit-cycle oscillations around $\phi_1 \approx 45$ deg, the oscillations break away to start oscillating around $\phi_1 \approx 18$ deg (note the change of ordinate scale at t = 20 s). However, in this case, the breakaway does not occur until after 37 oscillation cycles, compared to 12 for $\phi(0) = 72$ deg. The analytic tools developed in earlier analyses of a 65-deg delta wing[3,4,6] will be applied to unveil the flow mechanisms responsible for the roll-trim characteristics of the 60-deg delta wing exhibited in Figs. 1 and 2.

Analysis

At zero sideslip, β = 0, the roll-trim characteristics for the 60-deg delta wing[7] (Fig. 3) show similarities with those for the 65-deg delta wing[2,4] (Fig. 4). Thus, there are three trim points, ϕ_0 and $\pm\phi_1$. The static experimental characteristics for the 65-deg delta wing[1] are shown in Fig. 5. As discussed in Ref. 8, the measured $C_l(\phi)$ characteristics, although being highly nonlinear, are continuous rather than discontinuous, with the statically destabilizing data trend starting at $|\phi| = \phi_{cr}$. When $|\phi| > \phi_{cr} \approx 4$ deg, vortex breakdown moves very rapidly toward the trailing edge on the leeward, rising wing half. The associated statically destabilizing increase of the vortex-induced lift overpowers the statically stabilizing data trend generated by the vortex forward of vortex breakdown,[9] resulting in the measured $C_l(\phi)$ trend for $\phi_{cr} < |\phi| < \phi_d$. On the right, windward wing half, the vortex breakdown moves steadily forward toward the apex with increasing roll angle because of the associated decrease of the effective leading-edge sweep. The breakdown reaches the apex for $|\phi| \approx 13$ deg, according to the analysis in Ref. 5. The loss of vortex-induced lift on the windward wing half caused by this forward movement of the vortex breakdown augments the statically destabilizing data trend generated by the leeward wing half. Recent experimental results for a 60-deg delta-wing-body configuration[10] have revealed that when the breakdown of the windward vortex reaches the apex, the moderate suction generated by the lead-

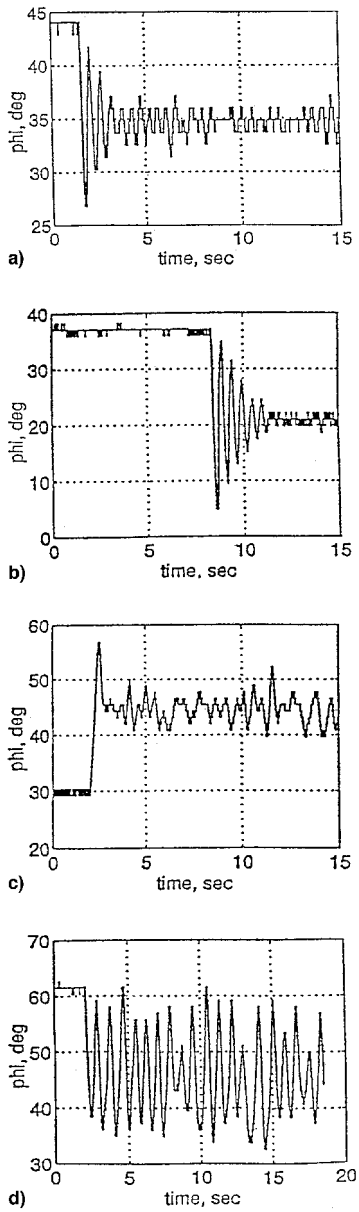

Fig. 1 Effect of sideslip on roll trim characteristics.[7] β = a) 0, b) 5, c) 10, and d) 15 deg.

ing-edge vortex downstream of a spiral type of vortex breakdown is wiped out. That is, the spiral leading-edge vortex is spilled downstream much as the leading-edge vortex in the case of dynamic airfoil stall.[11] For the 65-deg delta wing in Fig. 5, this statically destabilizing effect from the windward wing half most likely accounts for the experimental overshoot of the idealized characteristics at $\phi_d < \phi < \phi_s$, where $\phi_s \approx 13$ deg. At $|\phi| > \phi_s \approx 13$ deg, the windward wing half is completely stalled, contributing insignificantly to the rolling moment, whereas the leeward wing half generates the full, statically stabilizing, vortex-induced loading.[9] This caused the measured rapid decrease of the rolling moment for $\phi > 13$ deg, resulting in a stable trim point at $\phi_1 \approx 20$ deg. For roll perturbations around $\phi = 0$ at $\sigma = 30$ deg, where vortex breakdown caused by the effect of the fuselage[12] occurs back at 60% chord, the stabilizing vortex-induced loads forward of vortex breakdown dominate over the destabilizing effect of the roll-induced movement of the breakdown location. This produces the stable trim point at $\phi = 0$. At $|\phi| > \phi_{cr}$, however, the breakdown movement starts to dominate, generating the highly nonlinear, statically destabilizing data trend in Fig. 5.

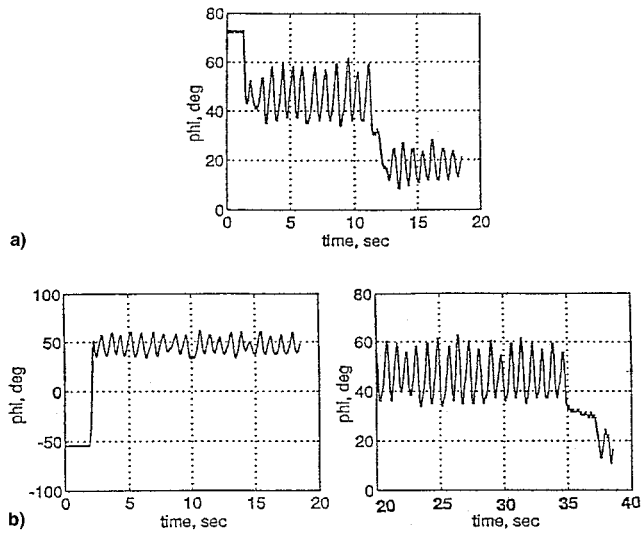

Fig. 2 Breakaway from one roll trim condition to another at β = 15 deg (Ref. 7). φ(0) = a) 72 and b) −52 deg.

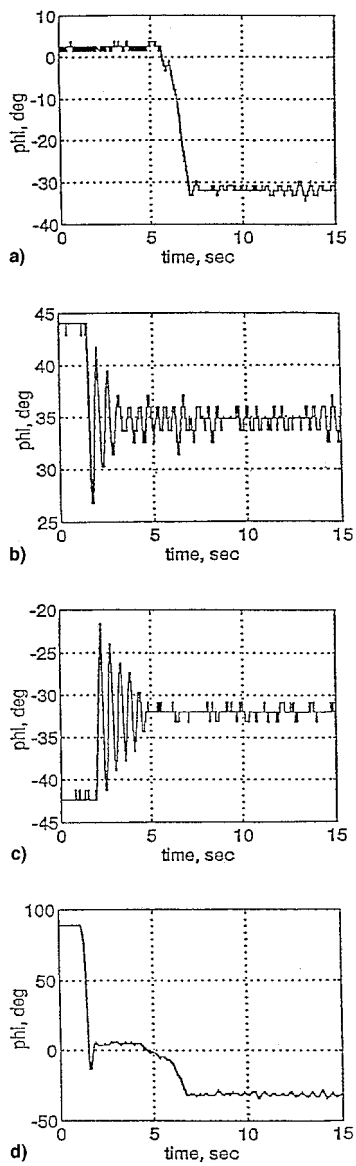

Fig. 3 Roll trim characteristics for 60-deg delta wing at β = 0 (Ref. 7). φ(0) = a) 2, b) 44, c) −32, and d) 90 deg.

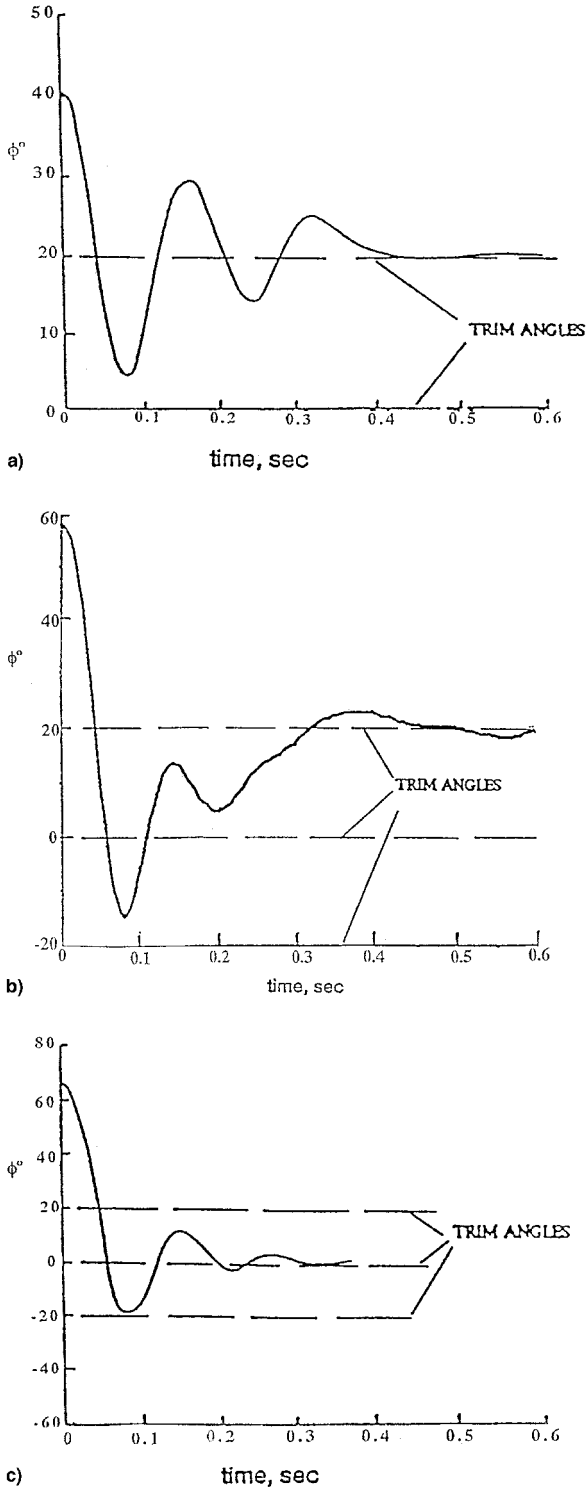

Fig. 4 Roll trim characteristics for 65-deg delta wing at β = 0 (Ref. 1). φ(0) = a) 41, b) 59, and c) 66 deg.

The idealized characteristics shown by a solid line in Fig. 5 were obtained by approximating the gradual movement of vortex breakdown from midchord to the trailing edge[13] (Fig. 6a) by a jumpwise movement. Accounting for the beveled leading edge,[14] this jump was expected to occur if the leading-edge sweep were increased from Λ = 65 deg to a value close to Λ = 70 deg; e.g., Λ ≈ 69 deg (Ref. 8). Figure 6b indicates that such a change of the sweep angle occurs on the left, leeward half of the 65-deg delta wing when the roll angle exceeds φ ≈ 7 deg. This value was used in Refs. 3 and 4 to construct

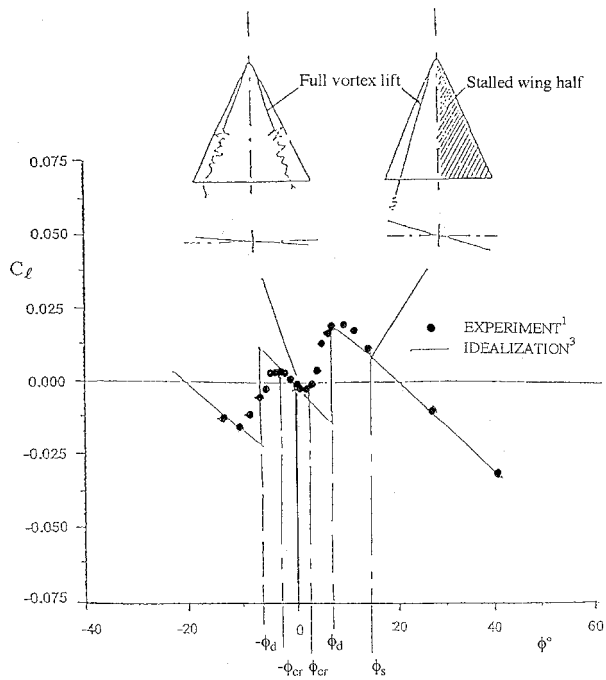

Fig. 5 Rolling moment characteristics for 65-deg delta wing at β = 0.

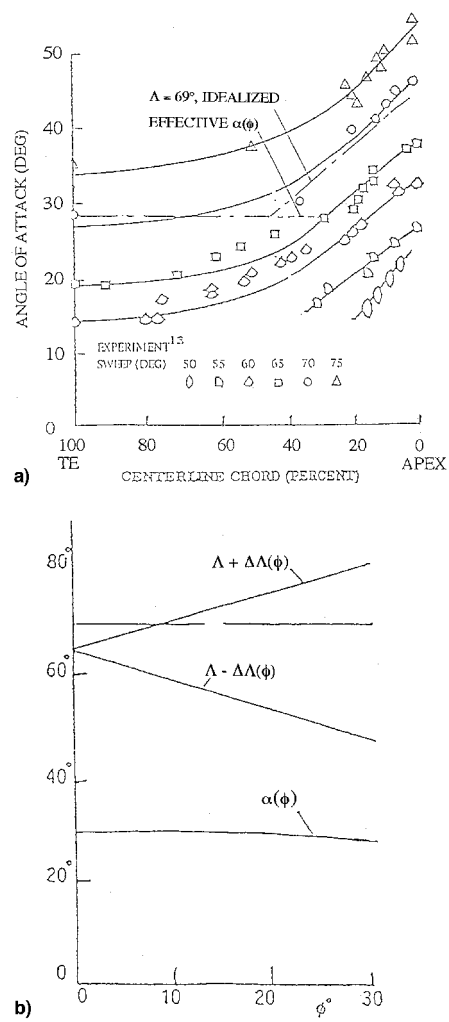

Fig. 6 Effect of roll angle on effective leading-edge sweep of 65-deg delta wing and the occurrence of vortex breakdown: a) $\xi_{VB} = f(\alpha, \Lambda)$, and b) α(φ) and Λ(φ) for σ = 30 deg.

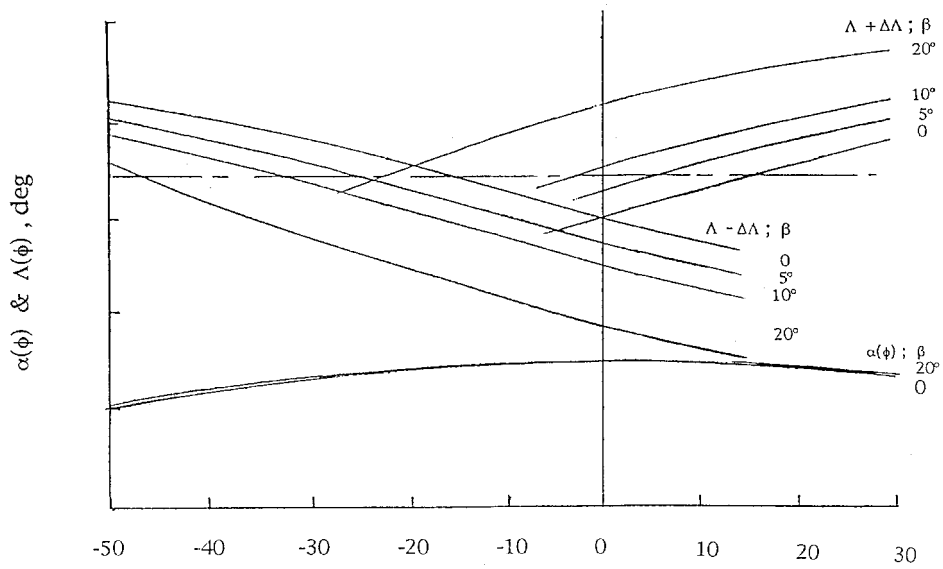

Fig. 7 Effect of sideslip and roll angle on effective leading-edge sweep and angle of attack of 60-deg delta wing.

the idealized $C_l(\phi)$ characteristics, shown by the solid line in Fig. 5.

When vortex breakdown on the leeward wing half (in the lateral sense) moves from midchord past the trailing edge, the regained vortex-induced lift generates a discontinuous, statically destabilizing change of the rolling moment. It is this flow phenomenon that is responsible for the appearance of the nonzero trim points $\phi_0 = \pm\phi_1$. The actual movement of the vortex breakdown is more gradual (Fig. 6a), resulting in experimental characteristics that are continuous rather than discontinuous (Fig. 5), with the statically destabilizing data trend starting at $\pm\phi_{cr}$ rather than at the discontinuity $\pm\phi_d$. However, as the idealized, discontinuous $C_\ell(\phi)$ characteristics have been shown to catch much of the important flow features,[3,4,6] they will be used here to unveil the essential flow physics associated with the observed roll-trim characteristics of a 60-deg delta wing at nonzero sideslip.

As illustrated by the flow sketches in Fig. 5 and discussed at length in Ref. 6, the rolling moment variation with ϕ for $|\phi| \leq \phi_d$ is determined by the movement of vortex breakdown on the leeward wing half-aft toward the trailing edge, and on the windward wing half-forward toward the apex. However, for $|\phi| > \phi_d$, the dominant contribution to the statically stabilizing rolling moment comes from the leeward wing half with its full vortex-induced loading. As the windward wing half has unorganized, fully separated flow for $|\phi| > \phi_s$, its contribution to the rolling moment is insignificant. Thus, the $C_l(\phi)$ characteristics for $|\phi| < \phi_s$, which determine the trim points $\pm\phi_1$, are essentially generated by the leeward wing half. According to earlier analyses,[9,15] the effect of sideslip can be accounted for by treating windward and leeward wing halves as parts of two delta wings at $\beta = 0$, with different leading-edge sweeps. This approach will also be used here. Consequently, the $C_l(\phi)$ characteristics of windward and leeward wing halves at $\beta \neq 0$ and $\phi \neq 0$ for the 60-deg delta wing will be obtained as the leeward and windward wing halves of two delta wings at $\beta = 0$, with their different leading-edge sweeps determined by β and ϕ. In addition, the combined effect of β and ϕ on the effective angle of attack of the wing halves has to be considered.

Effect of Sideslip

Expanding on the earlier definition of the effective leading-edge sweep[9,15] to include the effect of sideslip β, gives

$$\Lambda(\phi, \beta) = \Lambda \pm \tan^{-1}(\tan\sigma \sin\phi \sec\beta + \tan\beta \cos\phi \sec\sigma) \quad (1)$$

and the effective angle of attack becomes

$$\alpha(\phi, \beta) = \tan^{-1}(\tan\sigma \cos\phi \sec\beta) \quad (2)$$

For $\beta = 0$, Eqs. (1) and (2) produce the results shown in Fig. 6b for $\Lambda = 65$ deg and $\sigma = 30$ deg. Stephen[16] also used Eqs. (1) and (2) for $\beta = 0$ to correlate experimental results for vortex breakdown on delta wings with leading-edge sweeps in the range 45 deg $< \Lambda <$ 90 deg.

Figure 7 shows the effect of sideslip at $\sigma = 30$ deg for the 60-deg delta wing, where the effective leading-edge sweep $\Lambda(\phi, \beta)$, and angle of attack $\alpha(\phi, \beta)$, are determined by Eqs. (1) and (2), respectively. The figure shows how decreasing ϕ from a positive value gives a value for ϕ_d that decreases with increasing β, from $\phi_d \approx 16$ deg for $\beta = 0$, to $\phi_d \approx -22$ deg for $\beta = 20$ deg. In the ϕ_d that decreases with increasing β, from $\phi_d \approx 16$ deg for $\beta = 0$ to $\phi_d \approx -22$ deg for $\beta = 20$ deg. In the idealized case[3,4,6] used here, vortex breakdown jumps off the leeward wing half when ϕ_d is reached. For the other wing half, the windward side for $\beta > 0$, decreasing ϕ from positive to negative values to make this half the leeward wing half (in the lateral sense), makes ϕ_d go from $\phi_d \approx -16$ deg for $\beta = 0$, to $\phi_d \approx -47$ deg for $\beta = 20$ deg. In this case, vortex breakdown is also expected to jump off of the leeward wing half when ϕ_d is reached. However, for this to happen, a vortex with breakdown must exist on the wing half for $\phi > \phi_d$. Figure 7 shows that only for $\beta \leq 10$ deg is the wing sweep $\Lambda - \Delta\Lambda \geq 50$ deg for the windward wing half, and a vortex does exist at $\phi = 0$ (Fig. 6a), making it possible for the vortex breakdown to jump off the wing half at $\phi = \phi_d$. For $\beta = 20$ deg, effective sweep at $\phi = 0$ for the leeward wing half is less than 40 deg, and a leading-edge vortex in the usual sense does not exist. It may be possible for a vortex to develop at some $\phi > \phi_d$ also for $\beta = 20$ deg. However, in that case, the critical value $\Lambda = 69$ deg no longer applies, as the corresponding effective angle of attack $\alpha(\phi)$ is far below $\alpha = 30$ deg, approaching $\alpha = 20$ deg at $\phi = \phi_d$. The assumptions behind the idealized $C_l(\phi)$ characteristics, such as those shown in Fig. 5 for $\Lambda = 65$ deg, no longer apply when $\beta > 10$ deg and $\alpha(\phi_d, \beta) < 26$ deg. However, for $\beta \leq 10$ deg, the idealized $C_l(\phi)$ characteristics should provide guidance for the evaluation of the multi-roll-trim characteristics of the 60-deg delta wing.

Figure 7 shows that at $\phi = 0$ and $\beta = 5$ deg, the effective sweep of the leeward wing half of the 60-deg delta wing is slightly larger, but very close to that for the 65-deg delta wing at $\beta = 0$. Figure 8 shows in more detail how the leeward wing halves of the 65-deg delta wing at $\beta = 0$ and the 60-deg delta

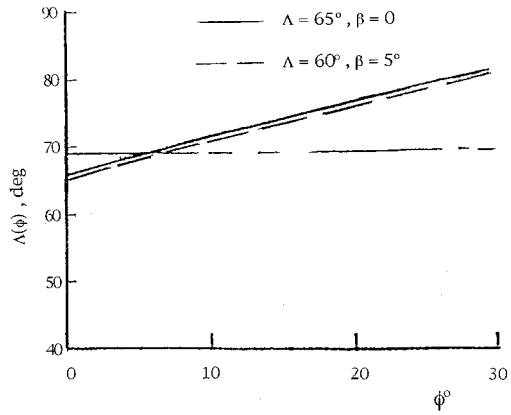

Fig. 8 Comparison between effective leading-edge sweep $\Lambda(\phi)$ for the leeward wing half of the 65-deg delta wing at $\beta = 0$ and the 60-deg delta wing at $\beta = 5$ deg.

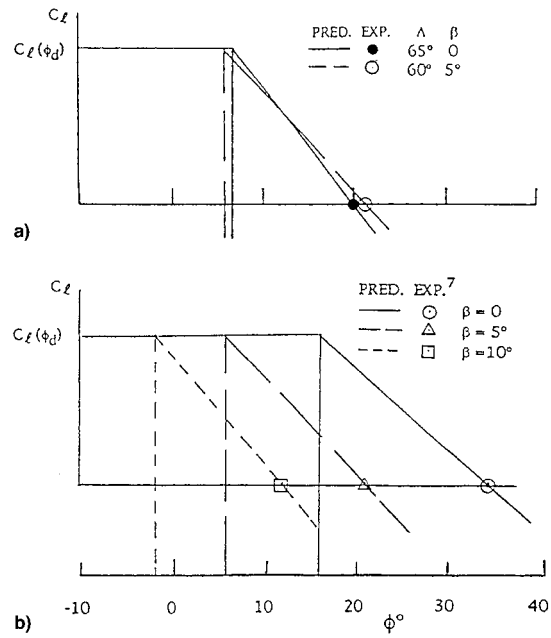

Fig. 9 Comparison effect of leading-edge sweep and sideslip on $C_l(\phi)$: a) $\Lambda = 65$ and 60 deg, and b) $\Lambda = 60$ deg and $\beta = 0$, 5, and 10 deg.

wing at $\beta = 5$ deg both give $\phi_d \approx 7$ deg. As the $C_l(\phi)$ characteristics at $\phi = \phi_d$ are essentially generated by the leeward wing half, one expects the $C_l(\phi)$ characteristics for the two wings to look as shown in Fig. 9a. From Figs. 7 and 8 one can see that $\alpha(\phi_d)$ for the two wings halves can hardly be distinguished from each other for $\phi > 0$, whereas they differ substantially for $\phi < 0$, with $\alpha(\phi_d) \approx 27$ deg at $\phi_d \approx -26$ deg for the 60-deg delta wing compared to $\alpha(\phi_d) \approx 30$ deg at $\phi_d \approx -7$ deg for the 65-deg delta wing. Even more important is the fact that the $C_l(\phi)$ characteristics for $\Lambda = 60$ deg near the trim point $\phi_1 \approx -47$ deg, where $\alpha(\phi_1) \approx 22$ deg, will be very different from those for $\Lambda = 65$ deg near the trim point $\phi_1 \approx -20$ deg, where $\alpha(\phi_1) \approx 28$ deg. Thus, the idealized $C_l(\phi)$ characteristics for the 60-deg delta wing at $\beta = 5$ and 10 deg are only applicable at $\phi > 0$, giving the results shown in Fig. 9b, where ϕ_d is the value obtained from Fig. 7 for $\Lambda = 69$ deg. The value $C_l(\phi_d)$ is that obtained for $\Lambda = 65$ deg and $\beta = 0$, which in turn came from Fig. 5. With $\Lambda(\phi_d)$ kept constant, and $\alpha(\phi_d) \approx 30$ deg, C_l is only a function of $(\phi - \phi_d)$, remaining very similar for the leeside wing halves at $\beta = 0$, 5, and 10 deg.

Studying the results in Fig. 6a and those in Fig. 7 for $\phi > 0$, one finds that the windward wing half will be stalled, either because vortex breakdown has moved to the apex or because the leading-edge sweep is to low to support a vortex, causing the wing half to have the aerodynamics of a moderately swept wing in deep stall. That is, the load variation with roll angle will be small and this wing half cannot contribute to the $C_l(\phi)$ characteristics in any significant way. The decrease of $\alpha(\phi_d)$ below 30 deg for $\beta < 0$ and $\beta > 10$ deg (Fig. 7) makes it difficult to apply the idealized $C_l(\phi)$ characteristics without access to static experimental $C_l(\phi)$ characteristics for the 60-deg delta wing. However, for $\beta = 0$, 5, and 10 deg, the idealized characteristics are well defined for the 60-deg delta wing using $C_l(\phi_d)$ for the 65-deg delta wing. This is demonstrated by Fig. 9b, where the predicted data points $[\phi_d, C_l(\phi_d)]$ are connected with the experimental trim points[7] $(\phi_1, 0)$.

Roll Oscillations Around Trim Points

Figure 10 summarizes the experimental results for the 60-deg delta wing,[7] not only showing the roll-trim-angle as a function of β, but also indicating whether the roll oscillations around the trim point were damped or not. For $0 \leq \beta \leq 10$ deg and $\phi_1 > 0$ in Figs. 7, 8, and 9, the performed analysis of a 65-deg delta wing[3,4,6] can help to supply the explanation for the damped nature of the roll oscillations. As mentioned earlier in the discussion of Fig. 5, for $\phi_{cr} < |\phi| < \phi_d$, the vortex breakdown on the leeward wing half moves rapidly from midchord past the trailing edge. This generates a statically destabilizing $C_l(\phi)$ trend and, through time–history effects,[17–20] contributes greatly to the damping of the roll oscillations around $\phi = 0$ for $|\phi| < \phi_d$ (Fig. 4). On the windward wing half, the undamping contribution of the unburst parts of the vortices forward of breakdown together with the downstream spiral vortices will together generate a rolling moment of lesser magnitude than that generated on the opposite wing half by the intact leading-edge vortex in the absence of vortex breakdown. As the unburst vortices cannot cancel the damping generated by potential flow over the rest of the 65-deg delta wing unless the angle of attack is increased above 45 deg, according to the theoretical results[9] in Fig. 11, the oscillations should be damped, in accordance with the experimental results in Fig. 4 for $\phi(0) = 66$ deg. A similar behavior would be expected of the 60-deg delta wing at $\beta = 0$. The tenuous character of the oscillations in this case for $\phi(0) = 2$ and 90 deg in Fig. 3 is the likely result of the close proximity to the apex of vortex breakdown for a 60-deg delta wing at $\sigma = 30$ deg and $\phi = 0$, $\beta = 0$ ($\alpha = 30$ deg in Fig. 6a). Thus, $|\phi_{cr}|$ is smaller than for the 65-deg delta wing, limiting the ϕ range over which static (and dynamic) stability can exist around $\phi = 0$.

For oscillations around the other trim points, $|\phi_1| > |\phi_d|$, the dominant contribution to the rolling moment comes from

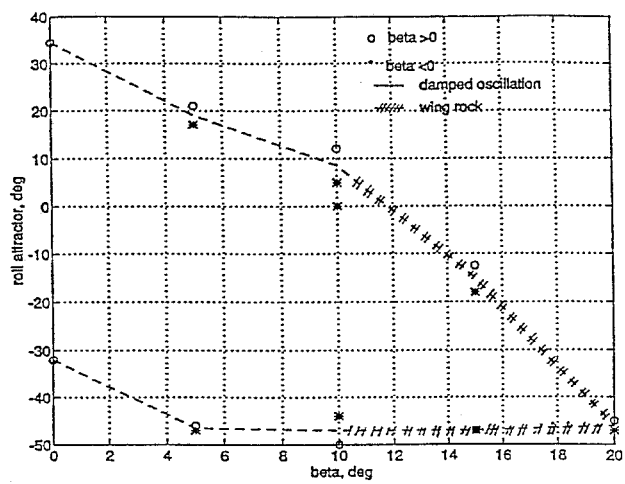

Fig. 10 Measured roll trim and observed nature of roll oscillations for 60-deg delta wing at $\sigma = 30$ deg (Ref. 7).

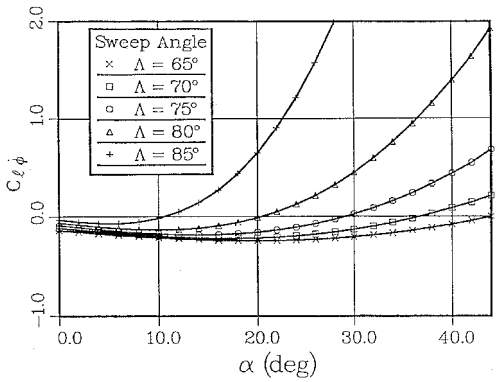

Fig. 11 Effect of leading-edge sweep on roll damping.[9]

the leeward wing half, as discussed earlier. Thus, the undamping contribution from the unburst leading-edge vortex becomes of concern. According to prediction[9] this will not result in undamped roll oscillations until a certain angle of attack has been exceeded (Fig. 11). For $\Lambda(\phi_d) = 69$ deg, Fig. 11 shows the critical angle to be $\alpha \approx 38$ deg. Thus, at $\sigma = 30$ deg, the roll oscillations should be damped for both the 65- and 60-deg delta wings (Figs. 4 and 3, respectively).

In Fig. 5, for $|\phi| \geq |\phi_d|$, the leeward wing half will contribute damping at $\alpha(\phi) \leq 30$ deg as long as $\Lambda(\phi, \beta) < 75$ deg (see Fig. 11). For the branches $\phi \geq \phi_d$ in Fig. 9b for the 60-deg delta wing, the leeward wing half fulfills the preceding requirement, explaining why the oscillations around the trim points are damped for $\beta = 0$, 5, and 10 deg (Figs. 3 and 10). For $\beta = 10$ deg and $\phi_1 \approx 12$ deg (Fig. 10), Fig. 7 shows that $\Lambda(\phi_1) \approx 76$ deg and $\alpha(\phi_1) \approx 30$ deg. According to Fig. 11, the oscillations should be neutrally damped, if anything, in agreement with the results for $\beta = 10$ deg in Fig. 1. The observed undamped roll oscillations for $\beta > 10$ deg (Fig. 10) are in accordance with expectations, as Fig. 7 shows $\Lambda(\phi_1)$ to exceed 76 deg when β is increased beyond $\beta = 10$ deg, which is predicted[9] to result in undamped oscillations at $\alpha = 30$ deg (Fig. 11).

Nonlinear Aerodynamics

Up to this point, the discussion of the roll oscillations has not considered the fact that the unsteady aerodynamics are highly nonlinear. The observed jumps in the wing rock time histories[7] (Fig. 2) will be shown to be the result of nonlinear aerodynamic effects caused by the roll-rate-induced conical camber[4] (Fig. 12, inset). Following the suggestion in Ref. 21, static tests were performed with sheet-metal models deformed to produce the roll-rate-induced camber.[22] The test results confirmed the predictions,[3] showing that the twisted-up side of the delta wing experienced later vortex breakdown than the opposite, twisted-down side. Thus, for positive roll rate, the rate-induced camber delays vortex breakdown on the downstroking and promotes it on the upstroking wing half. For $\bar{\dot{\phi}} = \dot{\phi}b/2U_\infty = 0.05$ of the large-amplitude roll oscillations,[1] this camber effect was large enough to prevent the breakdown from moving downstream of the trailing edge on the port wing and upstream of it on the starboard wing[1,4] (Fig. 12). This explains why the statically destabilizing $C_l(\phi)$ discontinuities of the idealized static characteristics never materialized under the dynamic conditions. The remaining differences between the $C_l(\phi)$ characteristics for $\bar{\dot{\phi}} = 0.05$ and 0 are primarily the result of the combined effects of time lag and roll-rate-induced apparent mass.[9] Figure 12 shows that at the $\bar{\dot{\phi}} = 0.05$ rate, the nonlinear $C_l(\phi)$ characteristics between $-\phi_1$ and $+\phi_1$ never materialized because of the large roll-rate-induced camber effect. There exists no rampwise change of roll angle for which $\phi_0 = 0$ can be reached, because the rate-induced camber (Fig. 12, see inset) remains of finite magnitude for $\bar{\dot{\phi}} \neq 0$. Only for an oscillatory change of the roll angle is it possible to reach

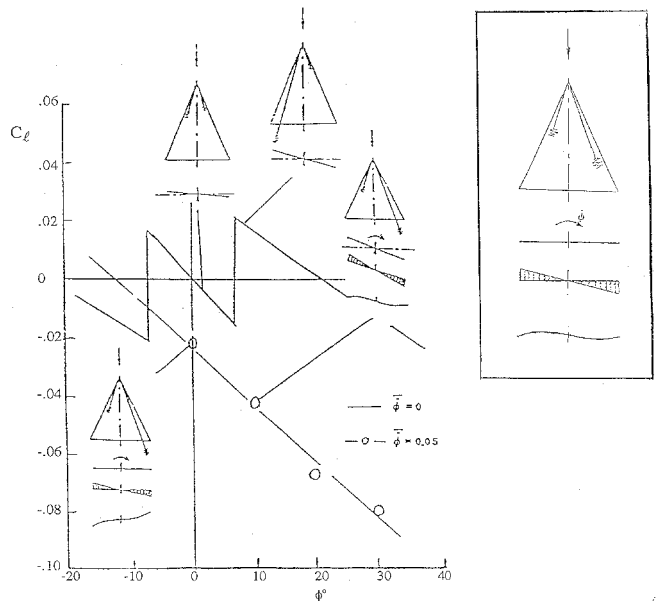

Fig. 12 Effect of roll-rate-induced camber on $C_l(\phi)$.[4]

$\phi_0 = 0$, and even then only with just the right roll-angle time–history; as in the case shown in Fig. 4 for $\phi(0) = 66$ deg, where the roll oscillations could enter and stay in the region $-\phi_{cr} < \phi < \phi_{cr}$, oscillating around the trim point $\phi_0 \approx 0$.

In Fig. 2, one can see examples of breakout from one established limit-cycle type of roll oscillation, commonly called wing rock,[19,20] to another oscillation around a different trim point. It is the effect of differences in past time histories that causes the observed differences in wing rock jumps.[7] This can be understood when studying the underlying flow physics.[6] The initial $\bar{\dot{\phi}}$ time histories are different; $\phi(0) = 72$ deg gives higher $|\bar{\dot{\phi}}|$ at $\phi_1 = 45$ deg than $\phi(0) = -52$ deg, explaining the earlier breakout for $\phi(0) = 72$ deg. Forced roll oscillations of the 65-deg delta wing[23] showed similarly large time–history effects.[3,4,6] The presence of ground-facility interference[24] could also cause a difference as a result of the different initial roll directions, decreasing ϕ for $\phi(0) = 72$ deg, increasing ϕ for $\phi(0) = -52$ deg.

The results discussed in the preceding text give food for thought in regard to the coupling existing between control demands and dynamic vehicle response[25] for advanced aircraft performing supermaneuvers.[26,27]

Conclusions

An analysis of the experimentally observed effect of sideslip on the unsteady aerodynamics of a 60-deg delta wing in free-to-roll oscillations around a 30-deg inclined axis has led to the following conclusions.

1) The roll dynamics are largely determined by the unsteady aerodynamics generated by the leeward (in the lateral sense) wing half.

2) Extension of analytic tools developed for the roll oscillations of a 65-deg delta wing provides the means needed for qualitative prediction of the roll-trim characteristics of a 60-deg delta wing at nonzero sideslip, including the nature of the roll oscillations (damped or undamped), as long as the effective angle of attack remains close to the inclination angle of the roll axis.

References

[1]Hanff, E. S., and Jenkins, S. B., "Large-Amplitude High-Rate Roll Experiments on a Delta and Double Delta Wing," AIAA Paper 90-0224, Jan. 1990.

[2]Hanff, E. S., and Ericsson, L. E., "Multiple Roll Attractors of a Delta

Wing at High Incidence," CP-494, AGARD, July 1991 (Paper 31).
[3]Ericsson, L. E., and Hanff, E. S., "Unique High-Alpha Roll Dynamics of a Sharp-Edged 65 Deg Delta Wing," *Journal of Aircraft*, Vol. 31, No. 3, 1994, pp. 520–527.
[4]Ericsson, L. E., and Hanff, E. S., "Further Analysis of High-Rate Rolling Experiments of a 65 Deg. Delta Wing," *Journal of Aircraft*, Vol. 31, No. 6, 1994, pp. 1350–1357.
[5]Jenkins, J. E., Myatt, J. H., and Hanff, E. S., "Body-Axis Rolling Motion Critical States of a 65-Degree Delta Wing," AIAA Paper 93-0621, Jan. 1993.
[6]Ericsson, L. E., "Flow Physics of Critical States for Rolling Delta Wings," *Journal of Aircraft*, Vol. 32, No. 3, 1995, pp. 603–610.
[7]Pamadi, B. N., Rao, D. M., and Niranjana, T., "Roll Attractor of Delta Wings at High Angles of Attack," International Council of the Aeronautical Sciences, 94-7.1.2, Sept. 1994.
[8]Ericsson, L. E., "Effect of Angle of Attack on Roll Characteristics of a 65-Degree Delta Wing," *Journal of Aircraft*, Vol. 34, No. 4, 1997, pp. 573–575.
[9]Ericsson, L. E., and King, H. H. C., "Rapid Prediction of High-Alpha Unsteady Aerodynamics of Slender-Wing Aircraft," *Journal of Aircraft*, Vol. 29, No. 1, 1992, pp. 85–92.
[10]Bergmann, B., Hummel, D., and Oelker, H.-C., "Vortex Formation over a Close-Coupled Canard-Wing-Body Configuration in Unsymmetrical Flow," CP-494, AGARD, July 1991 (Paper 14).
[11]Ericsson, L. E., and Reding, J. P., "Fluid Mechanics of Dynamic Stall, Part I, Unsteady Flow Concepts," *Journal of Fluids and Structures*, Vol. 2, No. 1, 1988, pp. 1–33.
[12]Ericsson, L. E., "Effect of Fuselage Geometry on Delta Wing Vortex Breakdown," AIAA Paper 97-0746, Jan. 1997.
[13]Wendtz, W. H., and Kohlman, D. L., "Vortex Breakdown on Slender Sharp-Edged Wings," *Journal of Aircraft*, Vol. 8, No. 3, 1971, pp. 156–161.
[14]Ericsson, L. E., and King, H. H. C., "Effect of Leading-Edge Cross-Sectional Geometry on Slender Wing Unsteady Aerodynamics," *Journal of Aircraft*, Vol. 30, No. 5, 1993, pp. 793–795.
[15]Ericsson, L. E., and Reding, J. P., "Approximate Nonlinear Slender Wing Aerodynamics," *Journal of Aircraft*, Vol. 14, No. 12, 1977, pp. 1197–1204.
[16]Stephen, E. J., Analysis of Rolled Delta Wing Flows Using Effective Sweep and Attack Angle," *Journal of Aircraft*, Vol. 32, No. 5, 1995, pp. 978–984.
[17]Ericsson, L. E. "The Fluid Mechanics of Slender Wing Rock," *Journal of Aircraft*, Vol. 21, No. 5, 1984, pp. 322–328.
[18]Ericsson, L. E., "Analytic Prediction of the Maximum Amplitude of Slender Wing Rock," *Journal of Aircraft*, Vol. 26, No. 1, 1989, pp. 35–39.
[19]Ericsson, L. E., "Slender Wing Rock Revisited," *Journal of Aircraft*, Vol. 30, No. 3, 1993, pp. 352–356.
[20]Ericsson, L. E., "Wing Rock Analysis of Slender Delta Wings, Review and Extension," *Journal of Aircraft*, Vol. 32, No. 6, 1995, pp. 1221–1226.
[21]Ericsson, L. E., "Analysis of Wind-Tunnel Data Obtained in High-Rate Rolling Experiments with Slender Delta Wings," National Research Council, Inst. for Aerospace Research, CR-14, Ottawa, ON, Canada, Aug. 1991.
[22]Hanff, E. S., and Huang, X. Z., "Prediction of Leading-Edge Vortex Breakdown on a Delta Wing Oscillating in Roll," AIAA Paper 92-2677, June 1992.
[23]Hsia, A. M., Myatt, J. H., and Jenkins, J. E., "Nonlinear and Unsteady Aerodynamic Responses of a Rolling 65-Degree Delta Wing," AIAA Paper 93-3682, Aug. 1993.
[24]Ericsson, L. E., and Beyers, M. E., "Ground Facility Interference on Slender Vehicle Dynamics," *Journal of Aircraft*, Vol. 33, No. 1, 1996, pp. 117–124.
[25]Ericsson, L. E., and Beyers, M. E., "Fluid/Motion Coupling in Conceptual Supermaneuvers," AIAA Paper 96-0787, Jan. 1996.
[26]Herbst, W. B., "Supermaneuverability," *Proceedings of the AFOSR/FJSRL/U. Colorado Workshop on Unsteady Separated Flows*, edited by M. S. Francis and M. V. Luttges, U.S. Air Force Academy, Colorado Springs, CO, 1983, pp. 1–9.
[27]Herbst, W. B., "Dynamics of Air Combat," *Journal of Aircraft*, Vol. 20, No. 7, 1983, pp. 594–598.